PFC/RR-91-10 DOE/PC-90350-3

DC CICC Retrofit Magnet Preliminary Design, Protection Analysis and Software Development

Quarterly Progress Report

Contract No. DE-FG22-90PC90350

J. Chen, P.G. Marston, J.R. Hale and A.M. Dawson

March 1991

Issued May 1991

Plasma Fusion Center

Massachusetts Institute of Technologyy

Cambridge, Massachusetts 02139, USA

This work was supported by the U.S. Department of Energy, Pittsburgh Energy Technology Center, Pittsburgh, PA 15236, under Contract No. DE-FG22-90PC90350. Reproduction. translation, publication, use and disposal, in whole or part, by or for the United States Government is permitted.

Magneto-Structural Analysis of a Preliminary Model for a DC CICC Retrofit Magnet using 2-D Orthotropic Finite Elements

1. Introduction

A previous model of this single dipole MHD magnet described in Report PFC/RR-91-7[1] indicated that a thin tension strap might be adequate for the superstructure. The stresses in windings, filler and tension strap were found to be within acceptable limits. However, the filler in the previous model occupied almost the same amount of space as the windings. The present model has been designed to use a minimum amount of filler, and to use it only between the windings and the tension strap. Figure 1 depicts half of the magnet cross section. The filler in the previous model has been, for the most part, replaced by windings, and the filler is now estimated to occupy only 1/9 of the space occupied by the windings. The tension strap is intended to be shaped to follow a funicular (momentless) curve. The degree of success in approaching the funicular curve will, however, be known accurately only after the analysis. This model represents the most recent iteration of the geometrical configuration of the windings developed to examine the corresponding change in stresses.

Another difference between this model and the previous one is the way in which the analysis is performed. The previous model used as the input the Lorentz force output from a stick model. The grid used in the stick model is transformed into the finite element grid. Each corresponding nodal point is identified and the associated Lorentz forces are applied. This process is rather time consuming. Software has been developed which uses finite elements to calculate the magnetic flux density from the known current density. The Lorentz forces are generated within the elements and are applied automatically to the

nodes. This eliminates the intermediate translations between different programs. It has required considerable time and effort to get these new codes working and verified, but they now represent a new and powerful analytical tool which greatly facilitates the iterative design process required for this exercise.

The third difference is that the previous analysis used isotropic material properties for the windings while, in this analysis, orthotropic properties are used. In addition, the effect of imperfect packing on the Young's moduli and Poisson's ratios of the windings is included.

2. Summary and Conclusion

The results indicate that imperfect packing of the windings may not affect the magnitudes and distributions of the global stresses in the tension strap, the filler, and the windings themselves. However, the magnitude and effect of local stress concentrations in the windings due to voids, which have not been included in this analysis, must be taken into consideration in a design. Although refinement in both the design and the finite element model will continue, the results achieved to date confirm the feasibility of a very efficient, low cost quasimomentless force containment structure for large-scale MHD dipole magnets.

3. The Assembly and Finite Element Mesh

Figure 2 shows the finite element mesh of a quadrant of the MHD magnet. The assembly includes 22 winding layers, each 0.04 m thick and wound on the X-Z plane, a tension strap, and some filler between the windings and the tension strap. Because of symmetry with respect to both the X=0 and Y=0 planes in structure, antisymmetry about the Y=0 plane and symmetry about the X=0 plane in the current direction, only a single quadrant needs to be analyzed. However, it is important that correct boundary conditions should be applied

along the X=0 and Y=0 planes. How these boundary conditions are identified and applied will be addressed in the section on analyses and results.

For simplicity suitable to a preliminary analysis, the magnet is assumed to be infinitely long in the Z direction. The geometry represents a cross section near the downstream end of the magnet bore. The field strength, however, is assumed to be 4.5 T. The analysis is thus conservative with respect to both structure and field uniformity. The "gap" between the tension strap and the filler in the previous model is kept and is also simulated by a thin (0.01 m thick) layer of an element with low Young's modulus. The structure is assumed to be continuous between the filler and the windings as well as between any two double pancakes.

The empty space enclosed within the tension strap and the space around the magnet are also modelled by finite elements. This is necessary to provide correct boundary conditions for a magnetic field analysis. These spaces are assumed to be filled by air. Figure 3 shows that air within a radius of 15.353 m from the center of the channel (the origin of the figure) is included in the model.

4. Magnetic Analysis and Results

The vector potential method is used in this analysis. Static magnetic fields are considered and the magnetic properties of air and all the materials in the magnet are assumed to be linear and isotropic. Under these assumptions, Maxwell's equations become:

$$\nabla \cdot \mathbf{B} = 0 \tag{1}$$

$$\nabla \times \mathbf{H} = \mathbf{J}, \tag{2}$$

where **B** is the magnetic flux density, **H** is the magnetic field intensity, and **J** is the current density. For linear isotropic media

$$\mathbf{H} = \frac{1}{\mu}\mathbf{B} \tag{3}$$

where μ is the absolute permeability of the medium. The magnetic vector potential **A** is selected such that

$$\nabla \times \mathbf{A} = \mathbf{B}, \tag{4}$$

in order for **B** to satisfy Eq. 1. Further simplification in Eq. 2, as is to be shown later, can be realized by choosing arbitrarily

$$\nabla \cdot \mathbf{A} = 0. \tag{5}$$

A vector such as **A** cannot be completely defined without specifying both its curl and divergence. It is assumed that the permeabilities for all media in this analysis are the same as in vacuum. That is

$$\mu = \mu_o = 4\pi \times 10^{-7} \quad (H/m). \tag{6}$$

Because **J** has only a Z component J_z, the X and Y components of magnetic vector potential **A** disappear, and the set of equations in the previous paragraph can be manipulated to reduce to the following one equation:

$$\nabla^2 A_z = -\mu J_z. \tag{7}$$

In the analysis, **J** is supplied and the assumption given in Eq. 6 is imposed. The potential **A** is obtained through Eq. 7, subject to the boundary conditions on **A**. The magnetic flux density **B** is then obtained through Eq. 4. The magnetic force per unit volume (body force density), which produces stresses, is obtained by

$$\mathbf{f_m} = \mathbf{J} \times \mathbf{B}. \tag{8}$$

For this analysis, the design magnetic flux density, **B**, at the center of the channel is

$$B_o = 4.5 \text{ T}. \tag{9}$$

In order to produce this field, a constant current density of

$$J_z = 13811000 \text{A/m}^2 \tag{10}$$

in the positive Z direction is applied to each element in the windings. Outside of a radius of 15.353 m (15 times the average dimension of the windings along the X axis) from the center of the channel, the magnetic flux density **B** is assumed to approach zero. In the case of zero flux density, the vector potential is a constant according to Eq. 4. It is thus convenient to choose

$$A_z = 0 \quad \text{at R} = 15.353 \text{ m}. \tag{11}$$

Because of symmetry in structure and antisymmetry in current direction, the field on the Y axis must have a Y component only. This means $B_x = \partial A_z/\partial y$ is zero, or A_z is constant, along the Y axis. According to Eq. 11, this means that

$$A_z = 0 \quad \text{along x} = 0. \tag{12}$$

Along the X axis, the field flux also has only a Y component due to symmetry in both structure and current direction with this axis. Therefore, $\partial A_z/\partial y = 0$ along the X axis. However, this condition is automatically satisfied by a stationary **A** and needs not be prescribed. In other words, there are no prescribed magnetic boundary conditions along the X axis.

The results of the magnetic analysis are shown in Figs. 4 through 9. Figures 4 and 5 show the flux density along the X and Y axes respectively. Clearly **B** approaches zero rapidly long before the distance from channel center reaches 15.353 m. Figure 6 shows constant **B** contours in the magnet winding and MHD channel. Figure 7 shows the plasma area within the channel on the midsection along the Z direction. It is required that flux density in this area be homogeneous within ±5%. Indeed, with the present design, the **B** is within +3% and -4% of the center field B_o. Figure 8 indicates the direction and relative magnitude of **B** in the magnet and its channel. Along both X and Y axes, **B** indeed has only a Y component, as required by the applied boundary conditions. Figure 9 shows the contours of constant **A** which have zero value along the Y axis and beyond 15.353 m from the channel center, as required by the boundary conditions.

5. Structural Analysis and Results

Among the important inputs for a structural analysis are the mechanical properties used for the materials. They are listed in Table 1. The air in the channel and around the magnet is not considered as part of the structure. It is not given any mechanical properties and is not allowed to deform (that is, there are no structural degrees of freedom assigned to it).

Because the magnet is symmetrical with respect to both X and Y axes, the structure cannot have the deformation components, v and u respectively, perpendicular to these two axes. That is

$$u = 0 \quad \text{along } x = 0, \tag{13}$$

and

$$v = 0 \quad \text{along } y = 0. \tag{14}$$

5.1 Perfectly packed orthotropic windings

The winding is a double pancake configuration as shown in Fig. 10. Approximate equivalent Young's moduli of the pancake can be estimated by using the following two equations for material in parallel and in series, respectively:

$$E_{eqp} = \sum f_{ip} E_i, \tag{15}$$

and

$$\frac{1}{E_{eqs}} = \sum \frac{f_{is}}{E_i}, \tag{16}$$

where f_{ip} and f_{is} are the volume fractions of the i^{th} material in the transverse and longitudinal directions, respectively.

The Young's modulus of the winding in the direction of the pancake thickness can be obtained in the following way: For simplicity, the round hole for superconductor can be approximated by a square hole with the same volume, as shown with dashed lines in Fig. 10. Let

r = radius of the original hole for superconductors,

t_h = half of the side length of the equivalent square area of the hole,

t_a = half of the side length of the aluminum square,

t_{ic} = thickness of the insulation wrap on a conduit,

t_{ip} = half of the insulation thickness between insulated conduits.

t_t = half of the side length of the conduit with all insulations,

E_a = Young's modulus of aluminum,

E_{ahip} = In-plane equivalent Young's modulus of aluminum square with a hole,

E_{ahop} = Out-of-plane equivalent Young's modulus of aluminum square with a hole,

E_{icf} = Through-thickness Young's modulus of insulation wrap for conduits,

E_{ipf} = Through-thickness Young's modulus of insulation between wrapped conduits,

E_{icc} = Crosswise Young's modulus of insulation wrap for conduits,

E_{ipc} = Crosswise Young's modulus of insulation between wrapped conduits,

E_{icl} = Lengthwise Young's modulus of insulation wrap for conduits,

E_{ipl} = Lengthwise Young's modulus of insulation between wrapped conduits,

E_{wf} = Young's modulus of winding in the thickness direction of the pancake,

E_{wc} = Young's modulus of winding in the width direction of the pancake,

E_{wl} = Young's modulus of winding in the longitudinal direction of the pancake.

The Young's modulus of the aluminum portion can be evaluated as follows: Since $(2t_h)^2 = \pi r^2$,

$$t_h = \frac{\sqrt{\pi}}{2} r. \tag{17}$$

Neglecting the contribution of superconductors in the hole and using Eqs. 15 and 16 , it can be shown that

$$\frac{1}{E_{ahip}} = \frac{t_h/t_a}{E_a(t_a - t_h)/t_a} + \frac{(t_a - t_h)/t_a}{E_a}, \tag{18}$$

and

$$E_{ahop} = \frac{t_a^2 - t_h^2}{t_a^2} E_a. \tag{19}$$

In the finite element model used (Fig. 2), the hole is not modeled. Instead, the aluminum conduit with a hole is modeled as a continuous medium. E_{ahip} and E_{ahop} are the equivalent Young's moduli of this medium.

The Young's modulus of the winding can be obtained by including the contributions from the insulators. Using Eqs. 15 and 16, it can be shown that

$$\frac{1}{E_{wf}} = \frac{t_a/t_t}{(t_a/t_t)E_{ahip} + (t_{ic}/t_t)E_{icc} + (t_{ip}/t_t)E_{ipc}} + \frac{t_{ic}/t_t}{E_{icf}} + \frac{t_{ip}/t_t}{E_{ipf}}, \tag{20}$$

and

$$E_{wl} = \frac{t_a^2}{t_t^2}E_{ahop} + \frac{(t_a + t_{ic})^2 - t_a^2}{t_t^2}E_{icl} + \frac{t_t^2 - (t_t - t_{ip})^2}{t_t^2}E_{ipl}, \tag{21}$$

where

$$t_t = t_a + t_{ic} + t_{ip}. \tag{22}$$

By symmetry

$$E_{wc} = E_{wf}. \tag{23}$$

According to the dimensions of Fig. 10 and the values from Table 1, we have

$$E_{wc} = E_{wf} = 39,900 \text{ MPa}, \tag{24}$$

and

$$E_{wl} = 55,200 \text{ MPa}. \tag{25}$$

It is also possible to evaluate the equivalent Poisson's ratios of the winding based on a model similar to that for the Young's moduli.
Let

ν_{wlc} = Poisson's ratio of windings coupling the contraction in the width direction of the double pancake due to the lengthwise (longitudinal direction of conduits) deformation.

ν_{wlf} = Poisson's ratio of windings coupling the contraction in the thickness direction of the double pancake due to the lengthwise deformation.

ν_{wcl} = Poisson's ratio of windings coupling the contraction in the length direction of the double pancake due to the widthwise deformation.

ν_{wfl} = Poisson's ratio of windings coupling the contraction in the length direction of the double pancake due to the thicknesswise deformation.

ν_{wfc} = Poisson's ratio of windings coupling the contraction in the width direction of the double pancake due to the deformation over the thickness.

ν_{wcf} = Poisson's ratio of windings coupling the contraction in the thickness direction of the double pancake due to the widthwise deformation.

ν_{iclc} = Poisson's ratio of wrapping insulation coupling the contraction in the crosswise direction of the insulation due to the lengthwise deformation.

ν_{iplc} = Poisson's ratio of insulation between wrapped conduits coupling the contraction in the crosswise direction of the insulation due to the lengthwise deformation.

ν_{iccf} = Poisson's ratio of wrapping insulation coupling the contraction in the flatwise direction of the insulation due to the crosswise deformation.

ν_{ipcf} = Poisson's ratio of insulation between wrapped conduits coupling the contraction in the flatwise direction of the insulation due to the crosswise deformation.

ν_{iclf} = Poisson's ratio of wrapping insulation coupling the contraction in the flatwise direction of the insulation due to the lengthwise deformation.

ν_{ipcf} = Poisson's ratio of insulation between wrapped conduits coupling the contraction in the flatwise direction of the insulation due to the lengthwise deformation.

Suppose a uniaxial stress is applied to a composite made of materials in parallel, such as along the longitudinal direction of a conduit array, then the Poisson's ratio which relates the contraction perpendicular to the bonded interfaces to the deformation along the bonded interfaces is given by the rule of

mixtures:

$$\nu_{wlc} = \frac{t_a^2 - t_h^2}{t_t^2 - t_h^2}\nu_a + \frac{t_{ic}t_t}{t_t^2 - t_h^2}\nu_{iclc} + \frac{t_{ip}t_t}{t_t^2 - t_h^2}\nu_{iplc} + \frac{t_{ic}(t_t - t_{ic} - t_{ip})}{t_t^2 - t_h^2}\nu_{iclf} + \frac{t_{ip}(t_t - t_{ic} - t_{ip})}{t_t^2 - t_h^2}\nu_{iplf}. \tag{26}$$

If, instead, the loading is applied perpendicular to the interfaces, the Poisson's ratio which relates the contraction along the interfaces due to a deformation perpendicular to the interfaces is obtained by assuming that the windings are orthotropic and from symmetry of the matrix modulus:

$$\frac{\nu_{wcl}}{E_{wc}} = \frac{\nu_{wlc}}{E_{wl}} \tag{27}$$

By geometrical symmetry,

$$\nu_{wlf} = \nu_{wlc}. \tag{28}$$

The Poisson's ratio which relates the in-plane contraction perpendicular to an in-plane deformation of the windings can be evaluated by combining the models provided in the two equations above. This gives

$$\nu_{wcf} = \frac{t_{ic}}{t_t}\nu_{iccf} + \frac{t_{ip}}{t_t}\nu_{ipcf} + \frac{t_a}{t_t}\left((t_a/t_t) * \frac{(1 - t_h/t_a)}{(1 + t_h/t_a - t_h^2/t_a^2)}\nu_a + (t_{ic}/t_t)\nu_{iccf} + (t_{ip}/t_t)\nu_{ipcf}\right) /$$

$$\left[(t_a E_{ahip} + t_{ic}E_{icc} + t_{ip}E_{ipc})\left(\frac{t_a}{E_{ahip}} + \frac{t_{ic}}{E_{icf}} + \frac{t_{ip}}{E_{ipf}}\right)\right]. \tag{29}$$

By geometrical symmetry,

$$\nu_{wfc} = \nu_{wcf}. \tag{30}$$

Taking $\nu_a = 0.29$, $\nu_{iclc} = \nu_{iplc} = 0.15$, $\nu_{iclf} = \nu_{iplf} = 0.3$, and $\nu_{iccf} = \nu_{ipcf} = 0.31$ from Table 1, the following Poisson's ratios are obtained for the windings:

$$\nu_{wlc} = \nu_{wlf} = 0.272, \tag{31}$$

$$\nu_{wcf} = \nu_{wfc} = 0.220. \tag{32}$$

The remaining two Poisson's ratios are obtained as follows:

$$\nu_{wcl} = \nu_{wfl} = \frac{E_{wc}}{E_{wl}}\nu_{wlc} = \frac{E_{wf}}{E_{wl}}\nu_{wlf} = 0.197. \tag{33}$$

5.2 Orthotropic windings with voids in bonding surfaces

This model is similar to that described in the previous section except that voids are assumed to exist in the interfaces between the conduit and the insulation and between insulators themselves. For simplicity in evaluating equivalent Young's moduli, it is assumed that these voids have a rectangular shape.

It is also possible to replace the insulation with a continuum which has smeared mechanical properties for the insulators and the voids, as we have already done for the aluminum in the previous section.
Let

$E_{I\parallel}$ = in-plane Young's modulus of insulation in the direction along the bonding surface,

$E_{I\perp}$ = in-plane Young's modulus of insulation in the direction perpendicular to the bonding surface,

E_{Il} = out-of-plane Young's modulus of insulation,

$E_{m\parallel}$ = in-plane smeared Young's modulus in the direction along the bonding surface,

$E_{m\perp}$ = in-plane smeared Young's modulus in the direction perpendicular to the bonding surface,

E_{ml} = out-of-plane smeared Young's modulus,

$f_{E\parallel}$ = ratio of the smeared Young's modulus to that of the insulation in the

direction along the bonding surface,

$f_{E\perp}$ = ratio of the smeared Young's modulus to that of the insulation in the direction perpendicular to the bonding surface,

f_{El} = ratio of the out-of-plane smeared Young's modulus to that of the insulation,

$f_{v\parallel}$ = fraction of length occupied by the voids in the direction along the bonding surface,

$f_{v\perp}$ = fraction of height occupied by the voids in the direction perpendicular the bonding surface.

Using a model similar to that for the aluminum, it can be shown that

$$\frac{1}{E_{m\perp}} = \frac{f_{v\perp}}{(1-f_{v\parallel})E_{I\perp}} + \frac{1-f_{v\perp}}{E_{I\perp}}, \tag{34}$$

$$E_{m\parallel} = (1-f_{v\parallel})E_{I\parallel}, \tag{35}$$

and

$$E_{ml} = (1-f_{v\perp}f_{v\parallel})E_{Il}. \tag{36}$$

Therefore,

$$f_{E\perp} = \frac{1-f_{v\parallel}}{f_{v\perp}+(1-f_{v\perp})(1-f_{v\parallel})}, \tag{37}$$

$$f_{E\parallel} = 1-f_{v\perp}, \tag{38}$$

and

$$f_{El} = 1-f_{v\perp}f_{v\parallel}. \tag{39}$$

Based on this model, the Young's moduli of the windings can be modified as follows:

$$\frac{1}{E_{wf}} = \frac{t_a/t_t}{(t_a/t_t)E_{ahip}+(t_{ic}/t_t)f_{E\parallel}E_{icc}+(t_{ip}/t_t)f_{E\parallel}E_{ipc}} + \frac{t_{ic}/t_t}{f_{E\perp}E_{icf}} + \frac{t_{ip}/t_t}{f_{E\perp}E_{ipf}}, \tag{40}$$

and

$$E_{wl} = \frac{t_a^2}{t_t^2} E_{ahop} + \frac{(t_a + t_{ic})^2 - t_a^2}{t_t^2} f_{El} E_{icl} + \frac{t_t^2 - (t_t - t_{ip})^2}{t_t^2} f_{El} E_{ipl}. \tag{41}$$

By symmetry

$$E_{wc} = E_{wf}. \tag{42}$$

For Poisson's ratios, it is directly from the rule-of-mixtures that

$$\nu_{wlc} = \frac{t_a^2 - t_h^2}{b^2}\nu_a + \frac{t_{ic} f_{v\perp} t_t f_{v\parallel}}{b^2}\nu_{iclc} + \frac{t_{ip} f_{v\perp} t_t f_{v\parallel}}{b^2}\nu_{iplc} + \frac{t_{ic} f_{v\perp} t_a f_{v\parallel}}{b^2}\nu_{iclf} + \frac{t_{ip} f_{v\perp} t_a f_{v\parallel}}{b^2}\nu_{iplf}, \tag{43}$$

where

$$b^2 = t_t^2 - t_h^2 - t_{ic} f_{v\perp} t_t f_{v\parallel} - t_{ip} f_{v\perp} t_t f_{v\parallel} - t_{ic} f_{v\perp} t_a f_{v\parallel} - t_{ip} f_{v\perp} t_a f_{v\parallel}. \tag{44}$$

Other Poisson's ratios can be obtained by obtaining the ratios of the Poisson's ratios for the equivalent insulators containing interfacial voids to the Poisson's ratios of the insulators. These ratios can be obtained by a straightforward consideration of stress and strain states in these two media. Therefore, only the results are to be stated.

Let

$f_{\nu_{cf}}$= ratio of ν_{cf} of equivalent insulation to that of the real insulation,

then

$$f_{\nu_{cf}} = \frac{1}{\frac{f_{v\perp}}{1 - f_{v\parallel}} + 1 + f_{v\perp}}. \tag{45}$$

Therefore,

$$\nu_{wcf} = \frac{t_{ic}}{t_t} f_{\nu_{cf}} \nu_{iccf} + \frac{t_{ip}}{t_t} f_{\nu_{cf}} \nu_{ipcf} +$$

$$\frac{t_a}{t_t}\left((t_a/t_t) * \frac{(1 - t_h/t_a)}{(1 + t_h/t_a - t_h^2/t_a^2)}\nu_a + (t_{ic}/t_t) f_{\nu_{cf}} \nu_{iccf} + (t_{ip}/t_t) f_{\nu_{cf}} \nu_{ipcf}\right) /$$

$$\left[(t_a E_{ahip} + t_{ic} E_{icc} + t_{ip} E_{ipc})\left(\frac{t_a}{E_{ahip}} + \frac{t_{ic}}{E_{icf}} + \frac{t_{ip}}{E_{ipf}}\right)\right]. \tag{46}$$

By geometrical symmetry,

$$\nu_{wfc} = \nu_{wcf}. \tag{47}$$

By assuming $f_{\nu\perp} = 0.286$ and $f_{\nu\parallel} = 0.35$ so that there is a 10% void fraction by volume in the insulations, we have

$$E_{wc} = E_{wf} = 34,900 \text{ MPa}, \tag{48}$$

$$E_{wl} = 54,500 \text{ MPa}, \tag{49}$$

$$\nu_{wlc} = \nu_{wlf} = 0.227, \tag{50}$$

and

$$\nu_{wcf} = \nu_{wfc} = 0.143. \tag{51}$$

5.3 Comparison of stress distributions with corresponding strengths

The stress distributions in the case of perfectly packed orthotropic windings are given in Figs. 11 through 15. The strengths of the materials in the magnet are given in Table 2. The comparison of these stresses and the corresponding strengths are summarized in Table 3. Figure 11 shows the distribution of X-component stresses in the windings. These stresses are compressive for most of the windings, as the windings are compressed by the magnetic body forces and by the reaction from the tension band. In general, along a constant Y line, the compressive stress increases in magnitude with X until the direction of magnetic force is reversed, then the magnitude decreases. The maximum compression exists at a corner of a double pancake which bears against the filler and has a magnitude of 18.6 MPa. The maximum tension is 31.7 MPa at the corner of a double pancake which separates from the filler. Tensile stresses in both the X and Y directions are an artifact of the finite element model which, at this stage of analysis, does not permit gap elements at interfaces which can support little or no tensile stress. The values are, however, useful because they indicate the level of compressive prestress required via the coil clamp to eliminate such gaps.

Figure 12 indicates the distribution of Y-component stress in the windings. Reactions from the tension band tend to bend the windings so that the surface

next to the channel is in compression while the surface near the tension band is in tension. However, the tension stress is reduced by the compressive magnetic body force in the Y direction. As a consequence, mild tension only occurs next to the tension band. In addition, compressive stress exists over most of the windings. The maximum compressive stress is 54 MPa. This occurs at the midsurface (Y=0) next to the channel. The maximum tensile stress is 11.7 MPa. This occurs on the surface near the tension band.

Figure 13 depicts the distribution of XY-component stress in the windings. This is the shear stress that tends to twist the conduits. It is apparent that the shear stress becomes greater as double pancake width decreases. The maximum shear stress in the present design is 13.7 MPa.

Because the strain is assumed to be zero in the Z direction as the cross section under examination is situated at the midlength of the MHD magnet, compressive stress is expected in the Z direction, as shown in Fig. 14. In addition to this normal stress, bending stress arises mainly due to the bending component of the Y-component stress. As a result, the maximum compressive stress occurs at the same location as that of the Y-component and is 13.9 MPa. The maximum tensile stress is only 5.4 MPa.†

Figure 15 shows the distribution of equivalent stress in the windings. This stress can be compared to the measured yield strength of the windings and can offer an estimate of possible yielding. The yield strength of the windings can also be estimated by the rule-of-mixtures. The maximum equivalent stress is 52.6 MPa.

In summary, the maximum tensile stress is 31.7 MPa, maximum compressive stress is 54 MPa, the maximum shear stress is 13.7 MPa, and the maximum equivalent stress in the windings is 52.6 MPa.

† Z-direction stresses from saddle forces are not yet included in the model.

The longitudinal stress along the straight portion of the tension band is quite uniform and is about 156 MPa. However, the bending component becomes unacceptably large where the tension strap bends into a curve. Previous analysis has shown that this stress can be reduced by increasing the radius of curvature in the high stress region. Modifications will be made on the next iterations to bring this stress concentration to within an acceptable level.

Finally, in Table 3, the stresses in the structural components of the magnet are compared with their corresponding strengths. The strengths are listed in parenthesis, while the factors of safety are given in square brackets. It is obvious that the yield strength in the tension strap has the smallest factor of safety, which is 1.6. However, the equivalent stress in the tension strap can be greatly reduced, if ample radius of curvature is provided to the curve of the strap. Redesign to reduce the stress in the high stress regions is under consideration.

References

[1] Marston, P. G., Chen, J., Hale, J. R., Dawson, A. M. (1991), "DC CICC Retrofit Magnet Preliminary Design, Protection Analysis and Software Development," PFC/RR-91-7, Plasma Fusion Center, MIT.

[2] "Handbook on Materials for Superconducting Machinery ," 1977 ed., Metals and Ceramics Information Center, Battelle Columbus Laboratories, Columbus, Ohio.

[3] Kasen, M. B., MacDonald, G. R., Beekman, Jr., D. H., and Schramm, R. E. (1980), "Mechanical, Electrical, and Thermal Characterization of G-10CR and G-11CR Glass-Cloth/Epoxy Laminates Between Room Temperature and 4 K," *Advances in Cryogenics Engineering (Materials)*, V. 26, pp 235-244.

[4] Markley, F. W., Hoffman, J. A., and Muniz, D. P., (1986), "Cryogenic Compressive Properties of Basic Epoxy Resin Systems," *Advances in Cryogenic Engineering Materials*, V. 32, pp 119-126.

Table 1

Young's moduli and Poisson's ratios of materials in the magnet

Material	E_{length} [1]	E_{cross} [2]	E_{flat} [3]	ν_{lc} [4]	ν_{cf} [5]	ν_{lf} [6]
Al [7]	70	70	70	0.29	0.29	0.29
G10CR [8]	28	22.4	11.2 [9]	0.15 [10]	0.31 [11]	0.30 [11]
Steel [12]	210	210	210	0.3	0.3	0.3
Epoxy [13]	4	4	4	0.3 [14]	0.3	0.3

Notes:

1. Lengthwise Young's modulus in GPa (this value and other values in the table is measured at room temperature).
2. Crosswise Young's modulus in GPa
3. Flatwise Young's modulus in GPa
4. Poisson's ratio coupling lengthwise and crosswise strains.
5. Poisson's ratio coupling flatwise and crosswise strains.
6. Poisson's ratio coupling lengthwise and flatwise strains.
7. Taken from Ref. 2.
8. Taken from Ref. 3.
9. Assumed to be half of E_{cross}.
10. From Ref. 3. The Poisson's ratio $\nu_{cl} = 0.144$.
11. Assumed values.
12. Taken from Ref. 2.
13. Young's modulus varies with curing agent added according to Ref. 4.
14. Value is 0.36 at 4 K, assume 0.3 at room temperature.

Table 2

Strengths of materials in the magnet

Material	tensile strength	compression strength	shear strength	yield strength
Al	490	490	–	445
G-10CR	415 $(\sigma_{IIt})^1$	375 $(\sigma_{IIc})^1$	60.1 $(\tau_{II})^1$	–
	257 $(\sigma_{Ict})^2$	283 $(\sigma_{Icc})^2$	45.2 $(\tau_{Ic})^2$	–
		420 $(\sigma_{Ifc})^3$	–	
Steel	1127	–	–	1027
Epoxy	100	–	–	–

Notes:

1. Lengthwise (wrap) strength in GPa (this value and other values in the table are measured at room temperature).
2. Crosswise (fill) strength in GPa
3. Flatwise (normal) strength in GPa

Table 3

Stresses and strengths of components in the magnet

Material	tensile [1] strength	compression strength	shear [3] strength	yield [4] strength
Tension strap				662 (1027) [1.6]
Windings	31.7 (100) [1] [3.2]	54.0 (420) [7.8]	13.7 (45.2) [3.3]	52.6 – –
Filler	12.4 (100) [8.1]	18.6 –	9.3 –	19.2 –

Notes:

1. Assume that the tensile strength of G-10CR is the same as the tensile strength of epoxy (this value and other values in the in table are measured at room temperature).

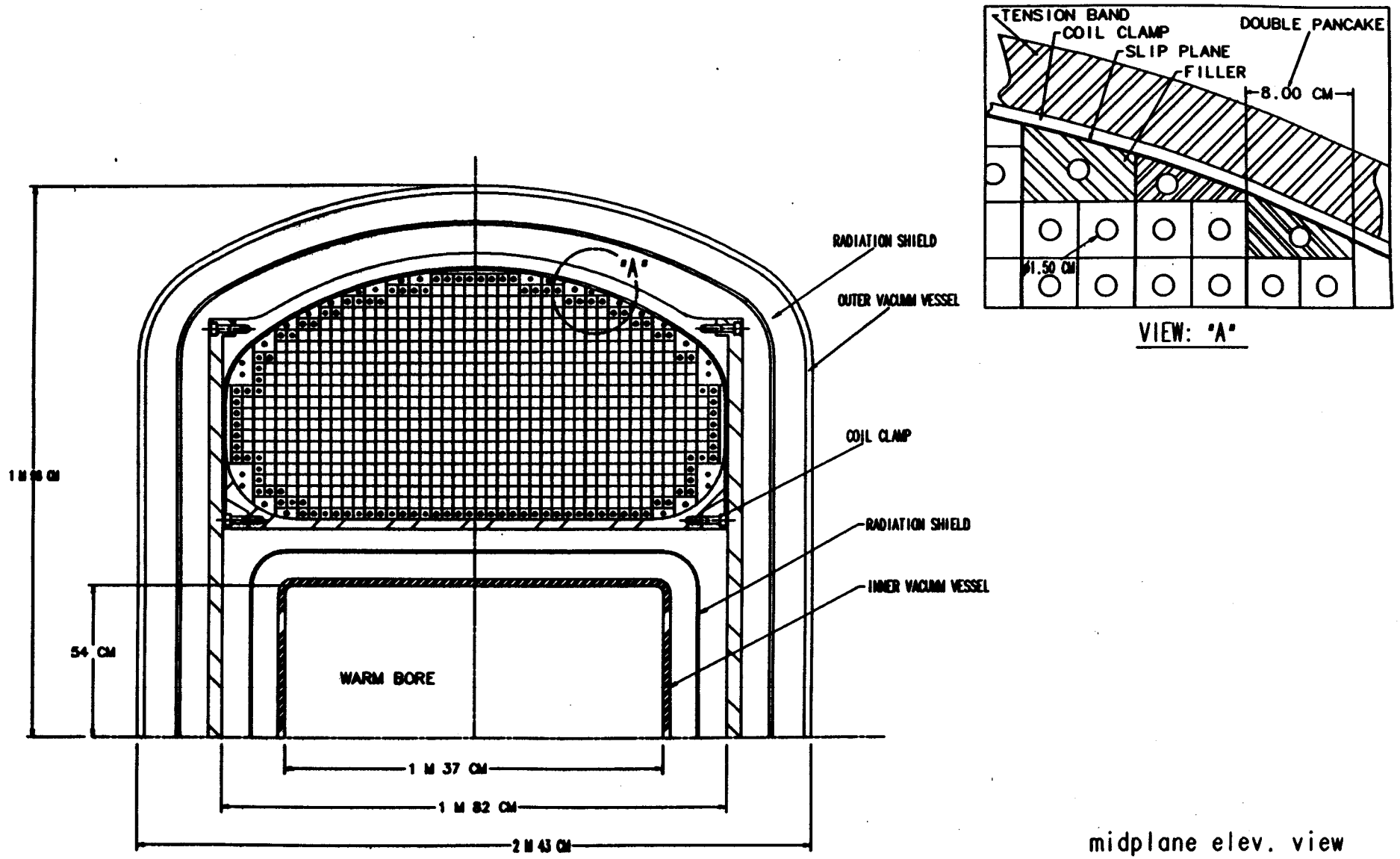

Figure 1 Cross Section of Coil Winding and Support

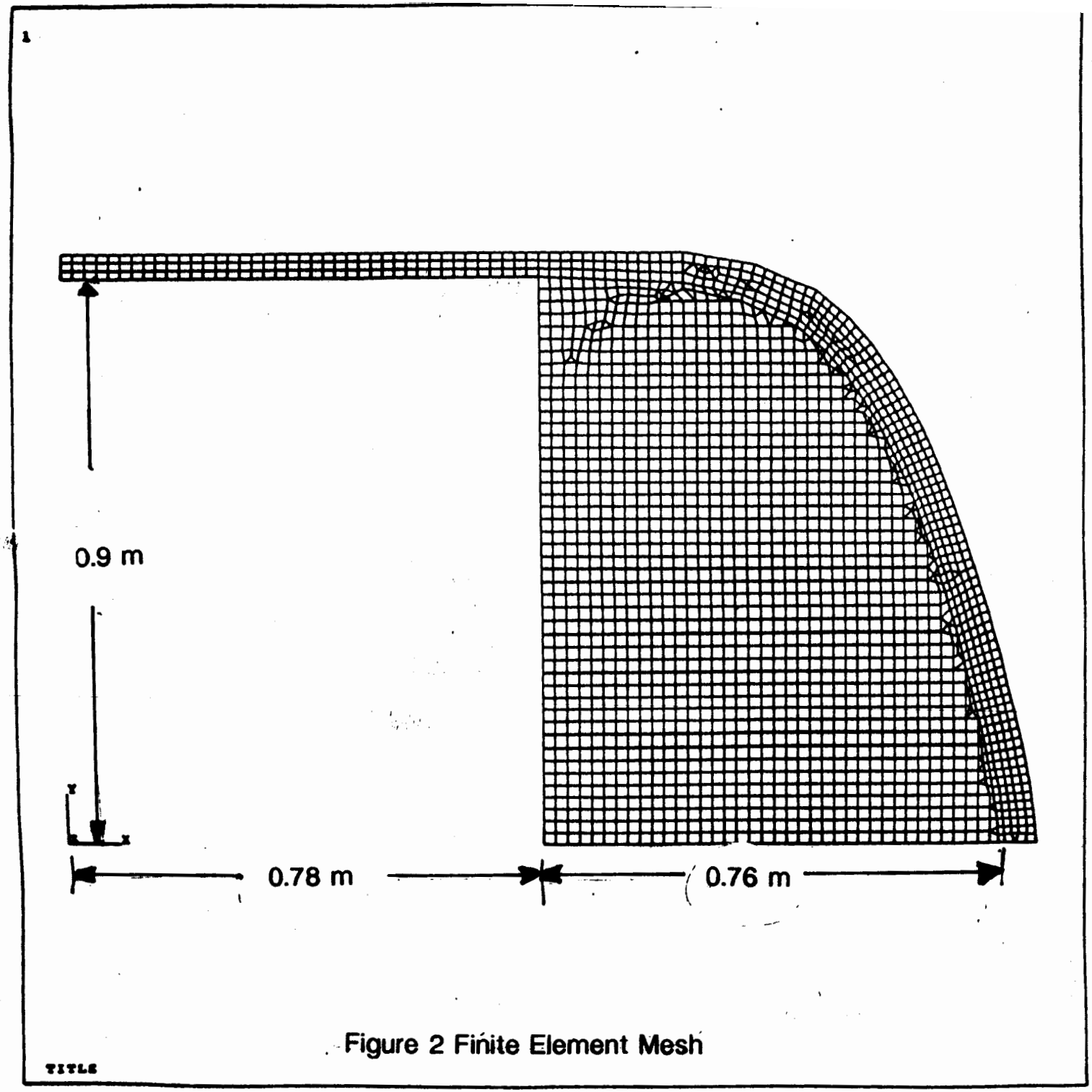

Figure 2 Finite Element Mesh

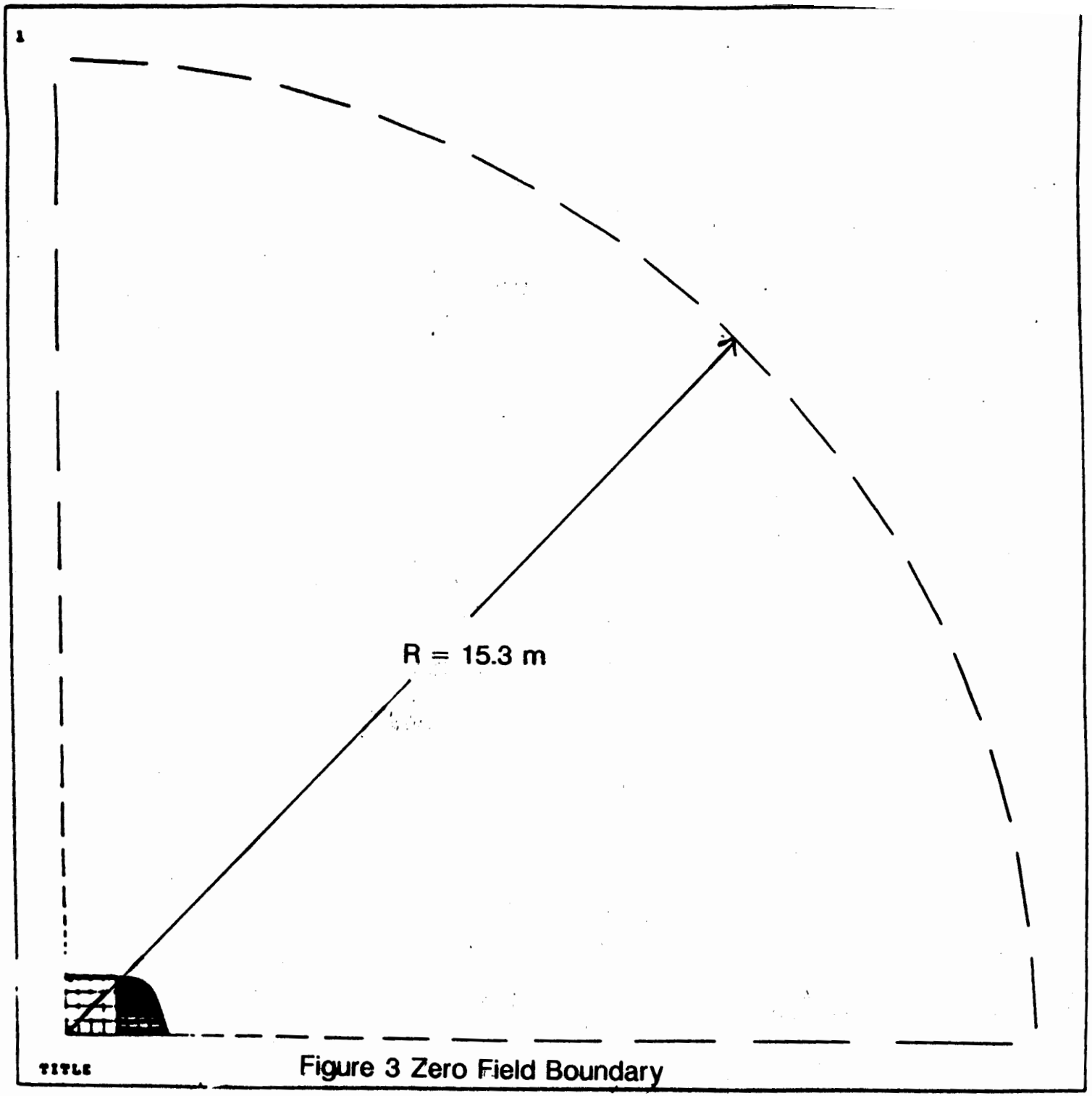

ANSYS 4.4A
MAR 22 1991
9:06:03
PLOT NO. 1
PREP7 AREAS
TYPE NUM

XV =1
DIST=8.444
XF =7.677
YF =7.677

Figure 3 Zero Field Boundary

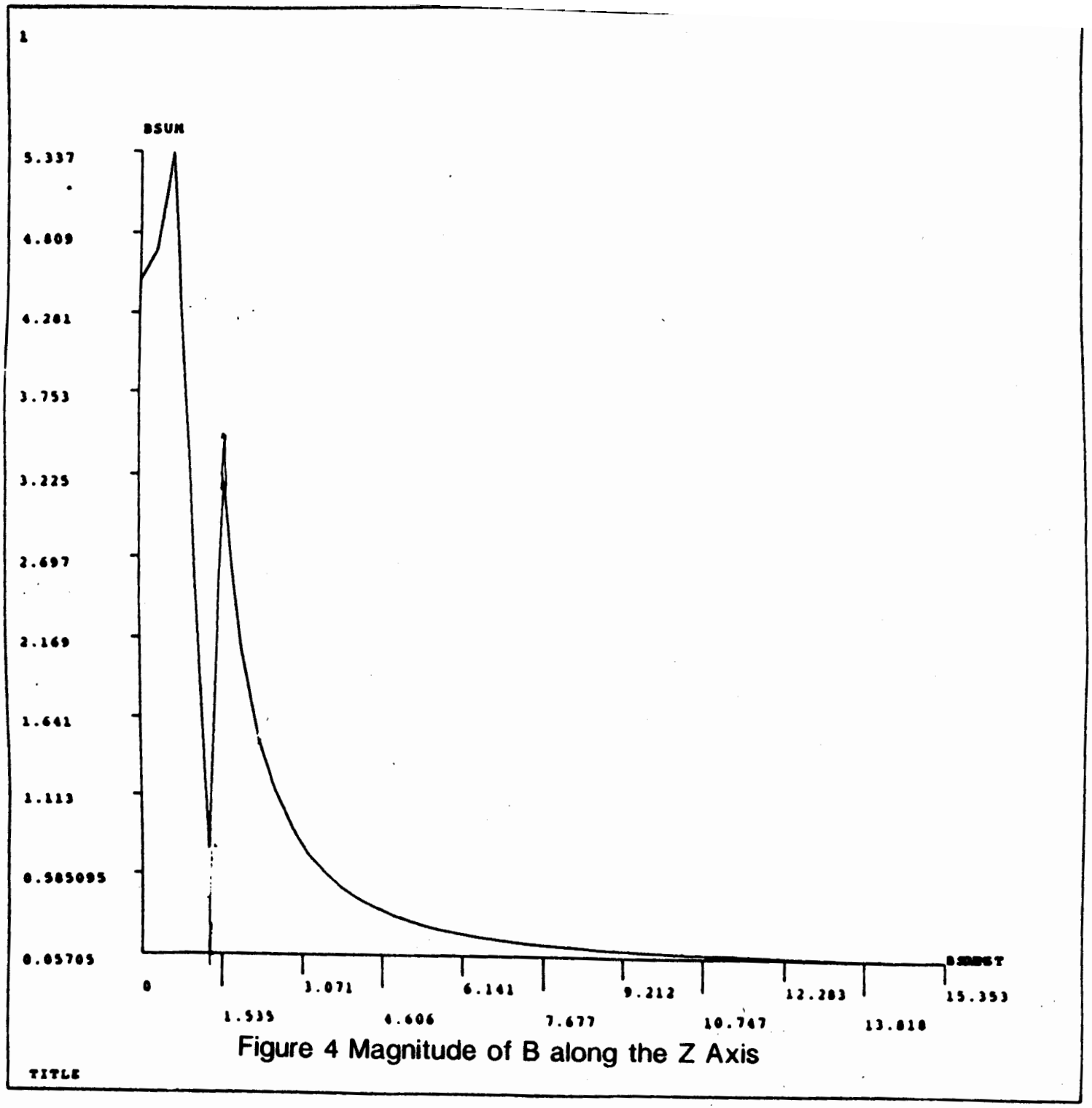

Figure 4 Magnitude of B along the Z Axis

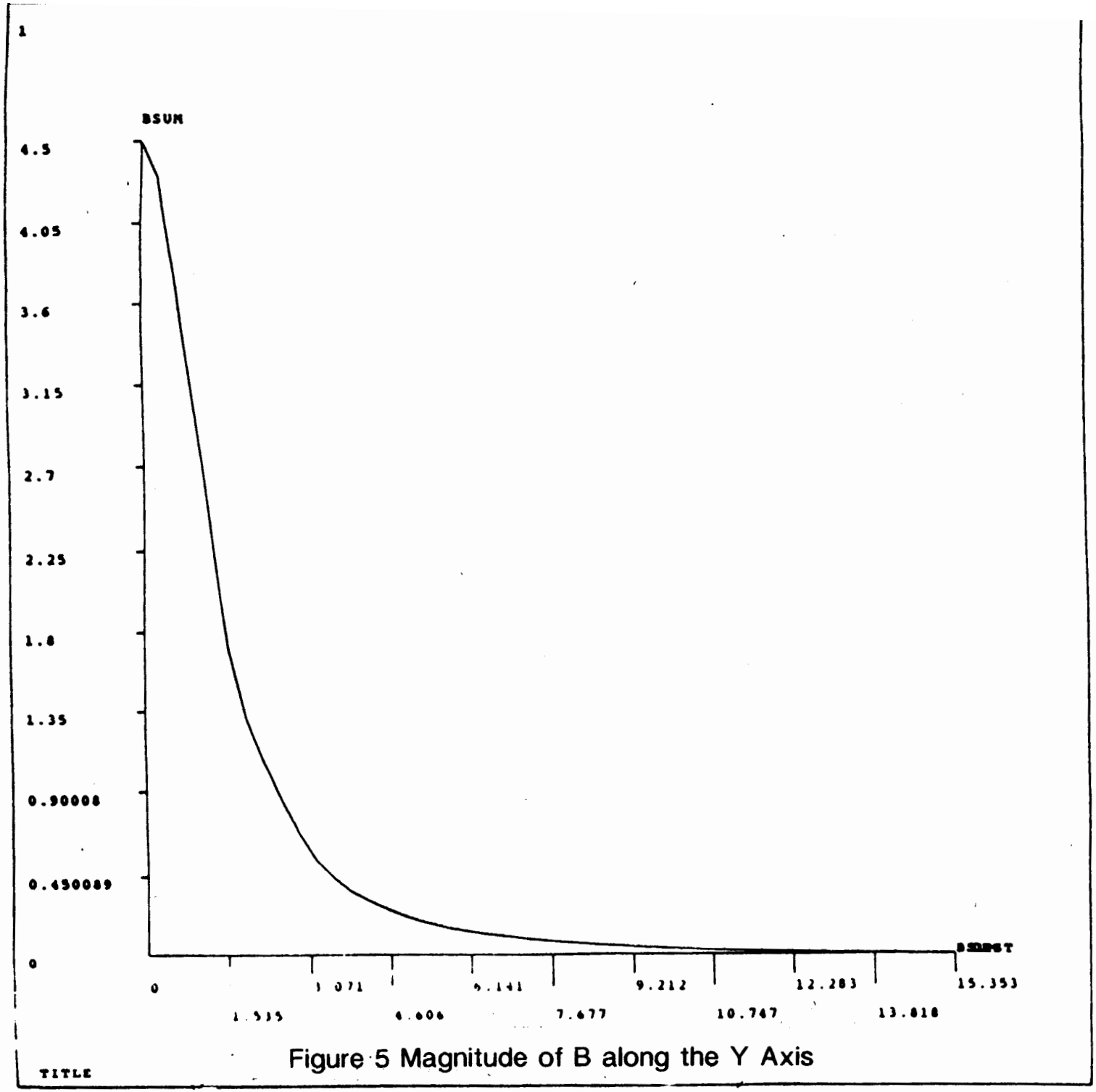

Figure 5 Magnitude of B along the Y Axis

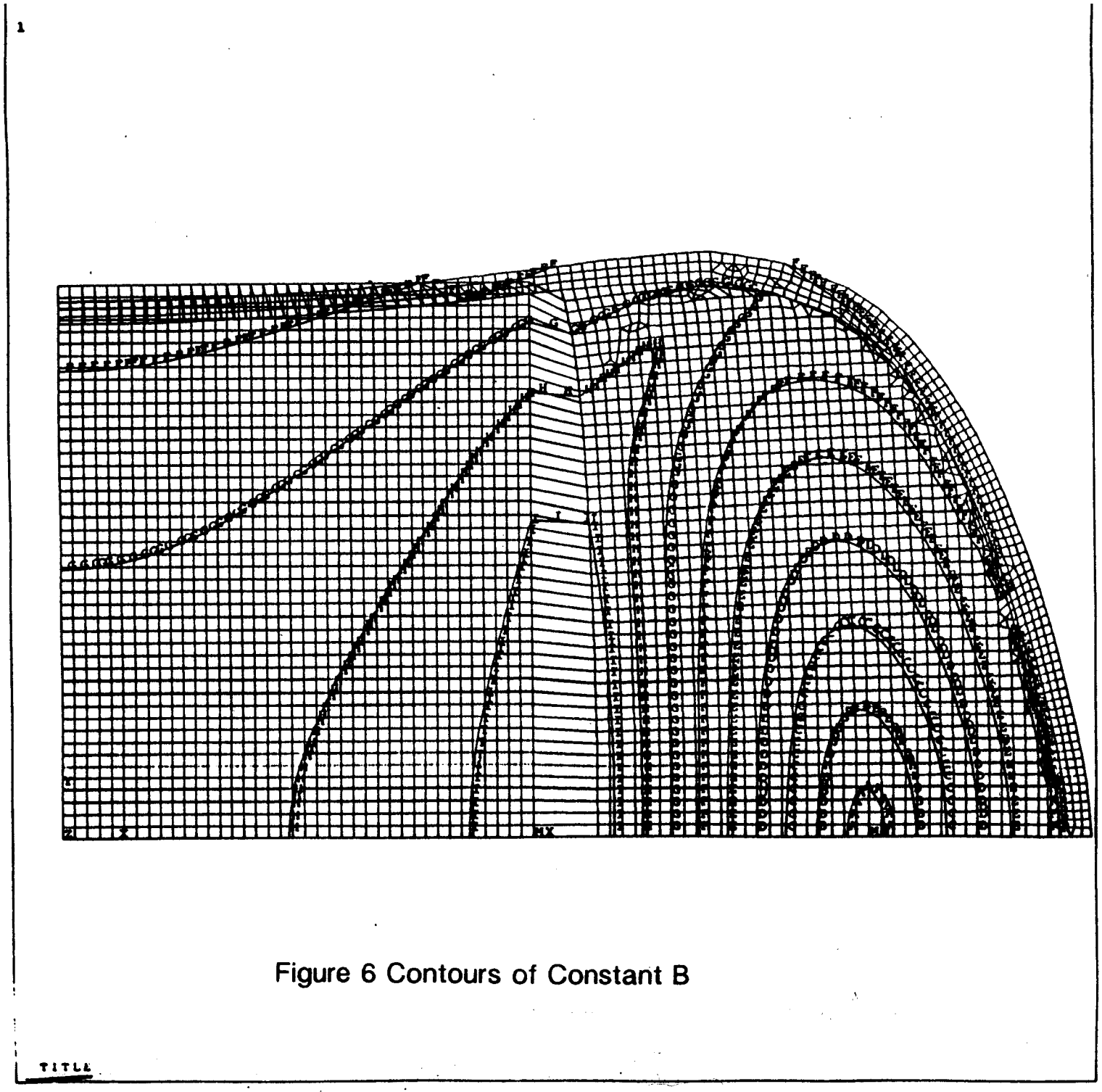

Figure 6 Contours of Constant B

Note: Deformation of the winding is greatly exaggerated

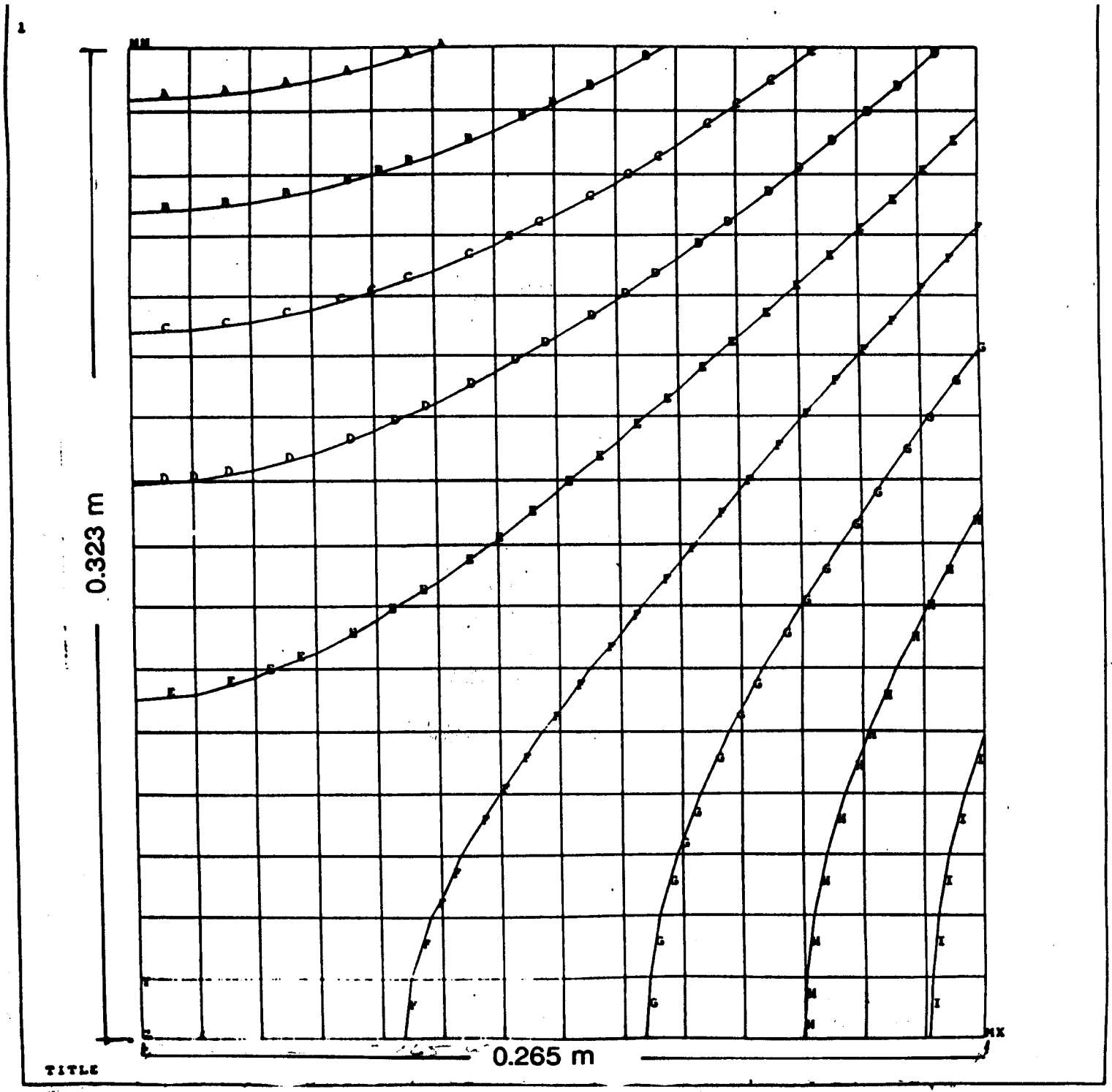

Figure 7 Contours of Constant B in Channel

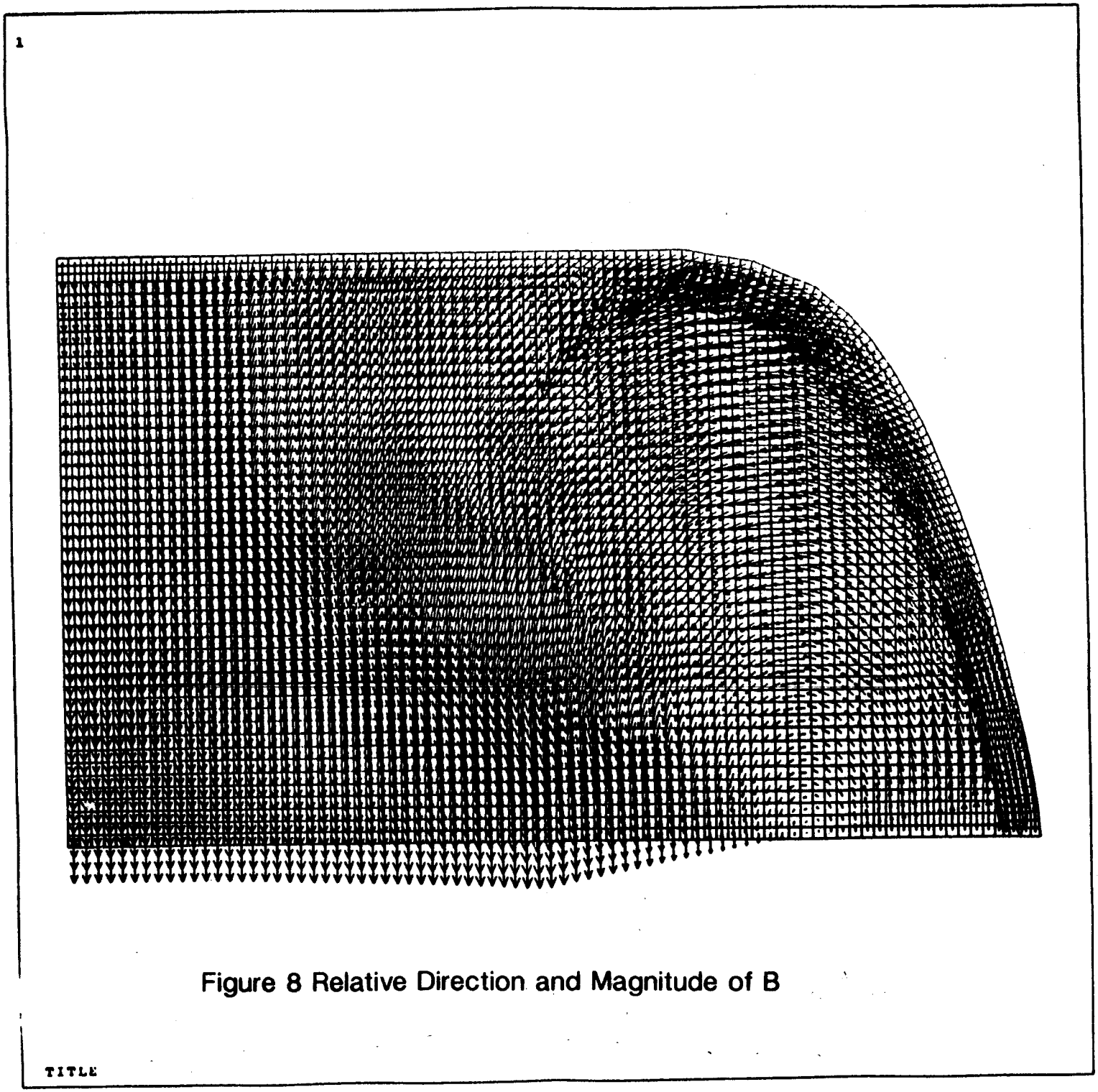

Figure 8 Relative Direction and Magnitude of B

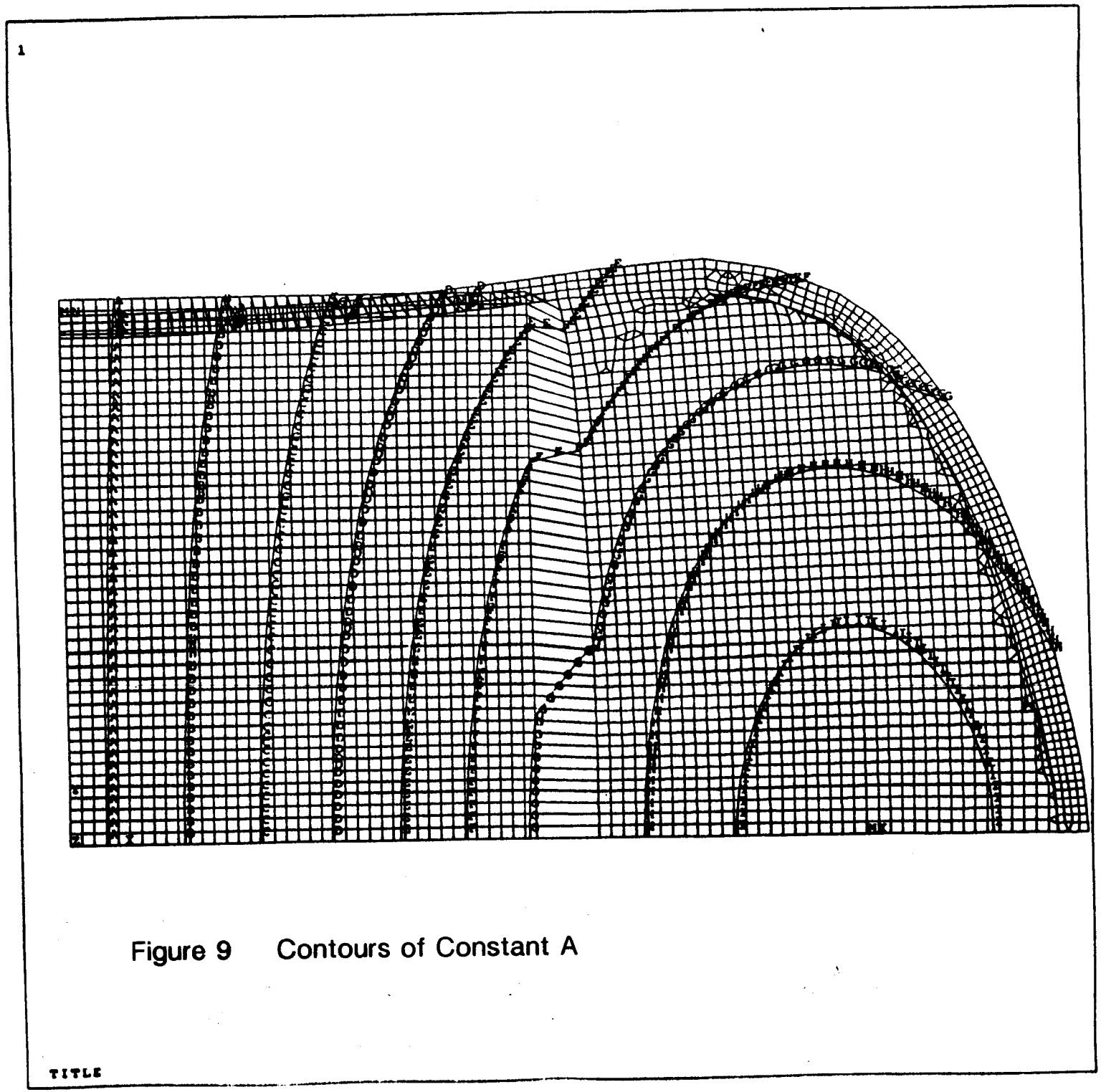

Figure 9 Contours of Constant A

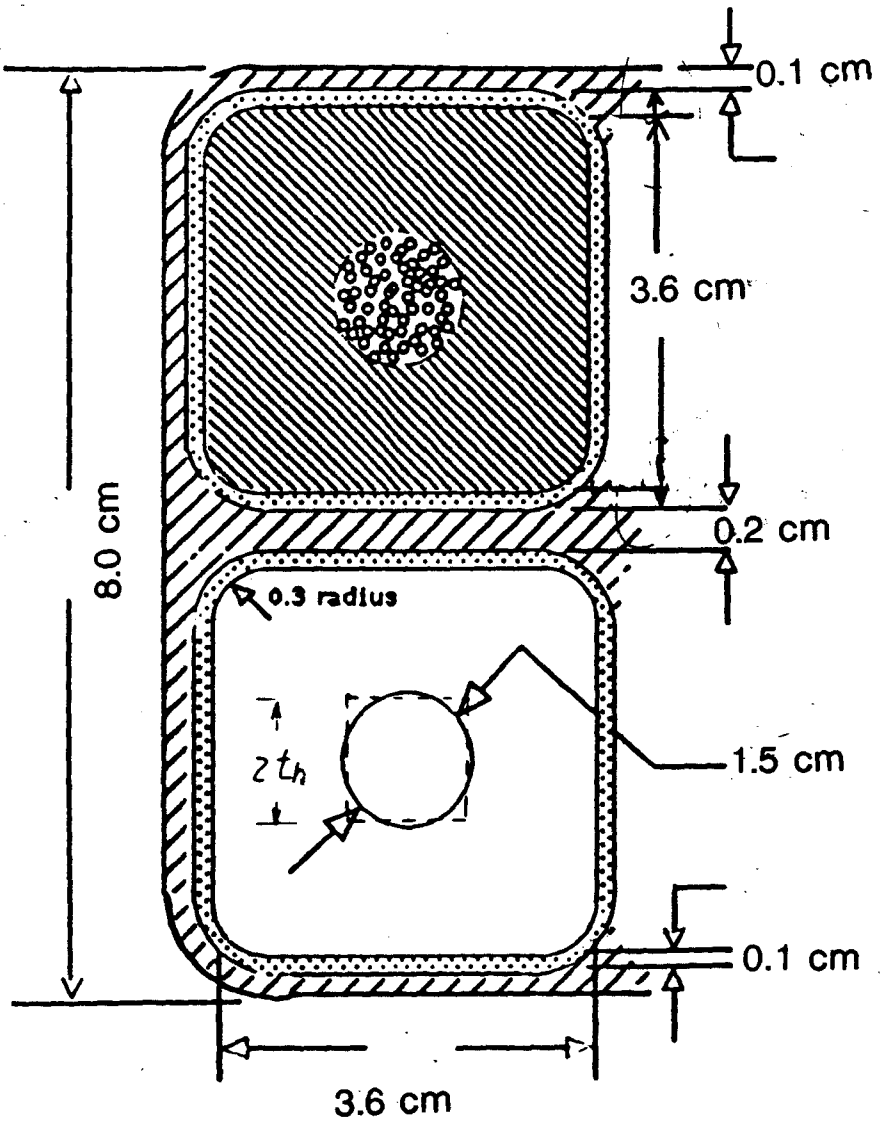

Figure 10 Double Pancake Configuration

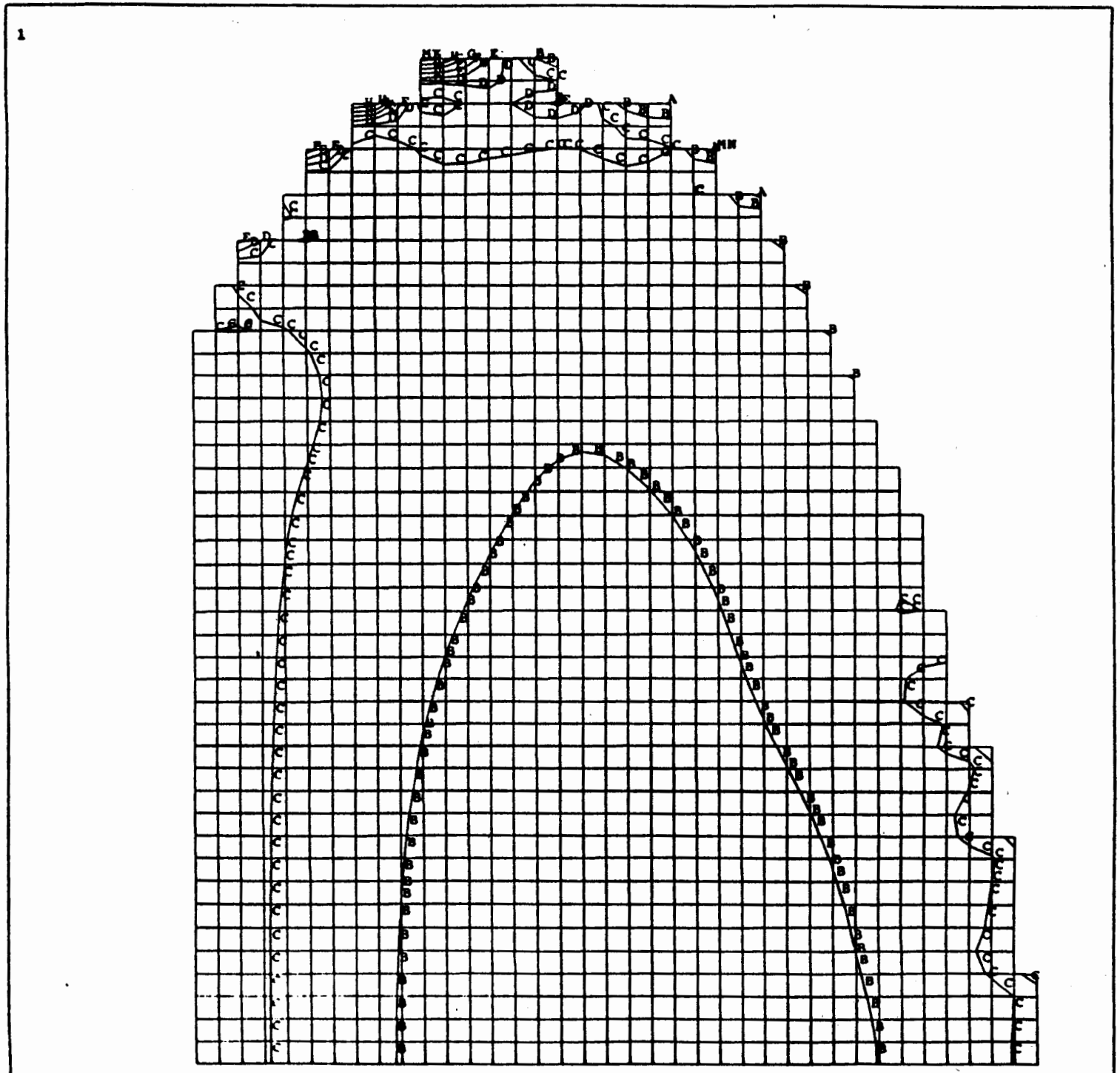

Figure 11 Distribution of the X Component of Stress

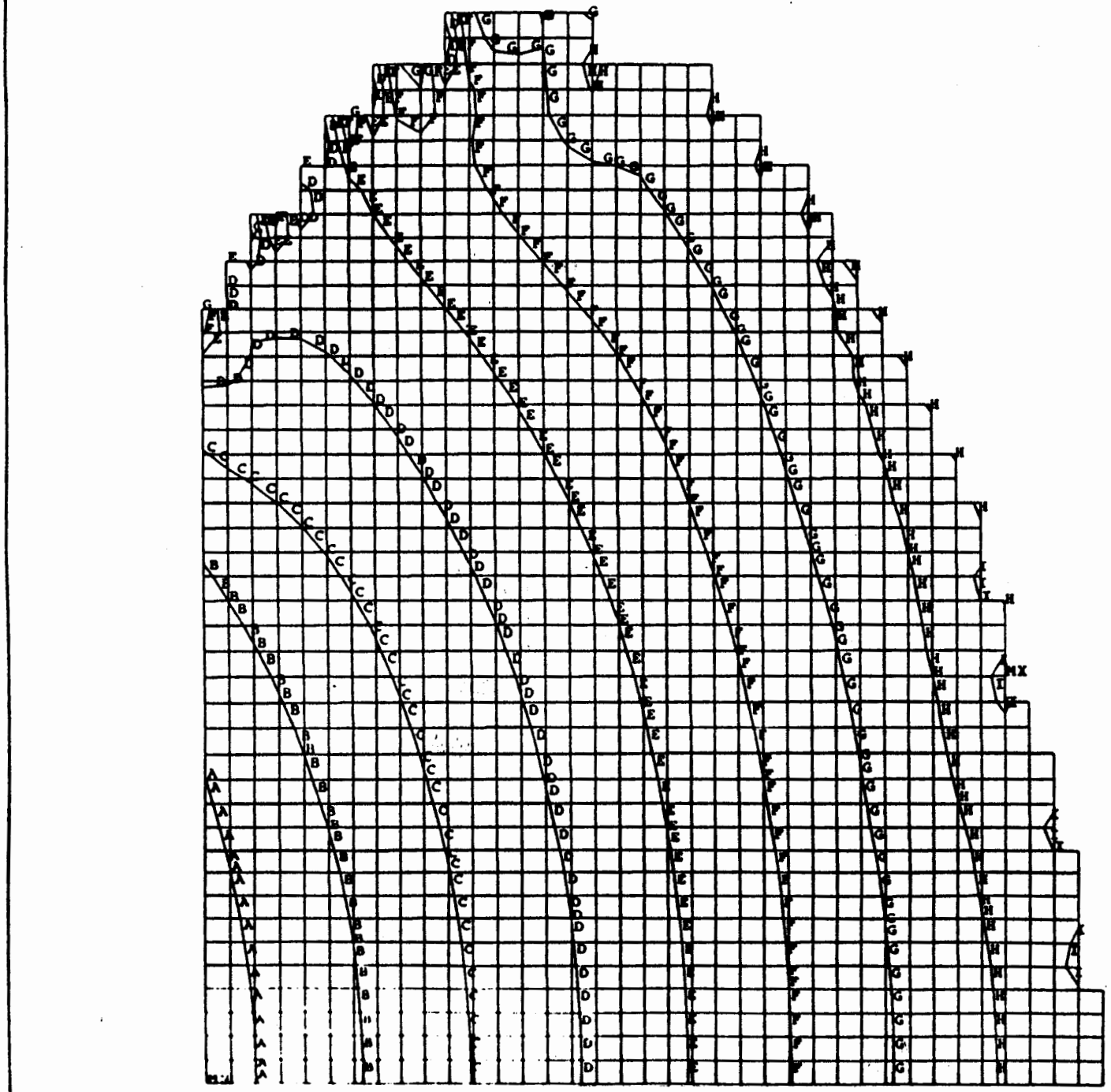

Figure 12 Distribution of the Y Component of Stress

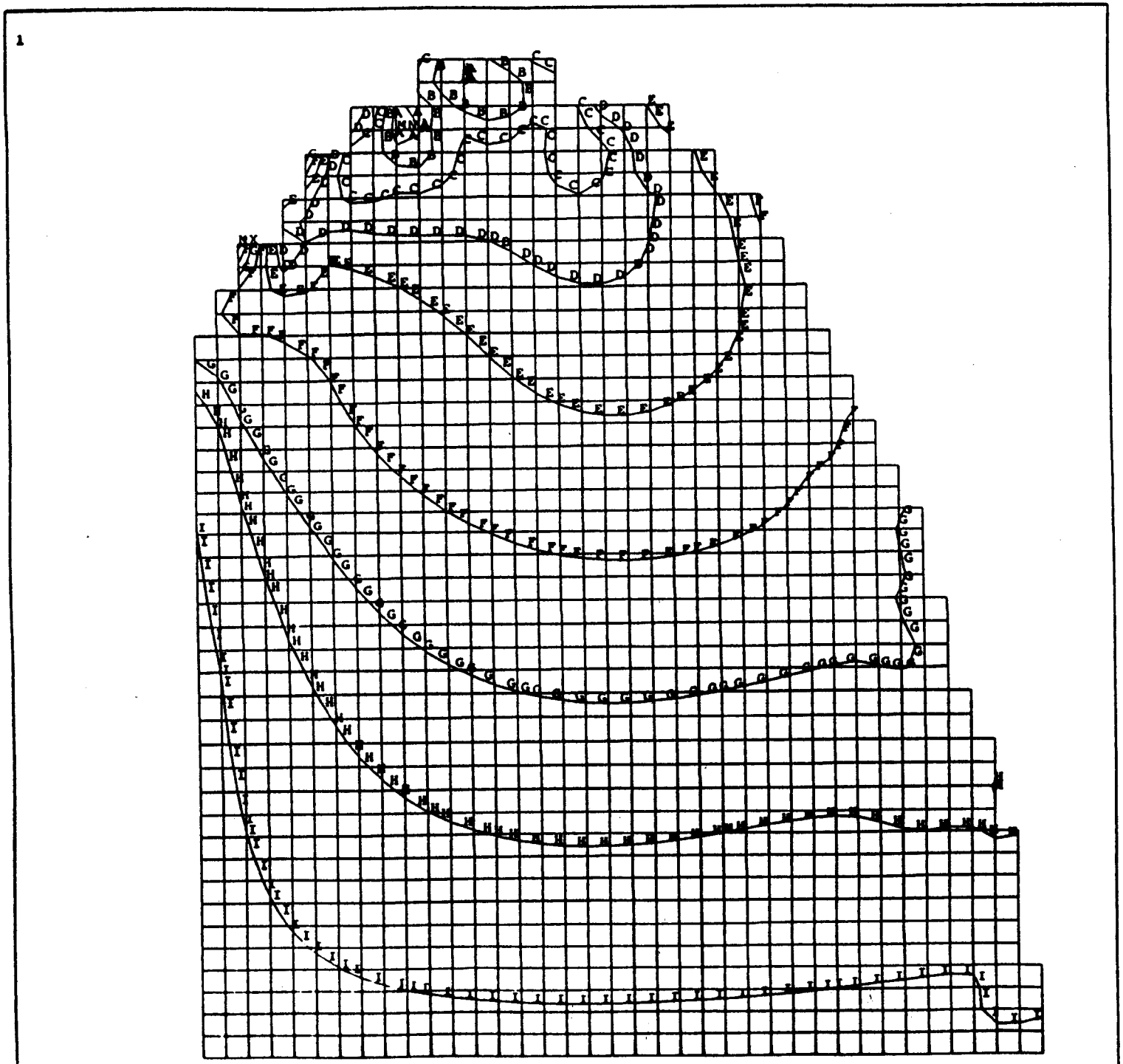

Figure 13 Distribution of X-Y Stress

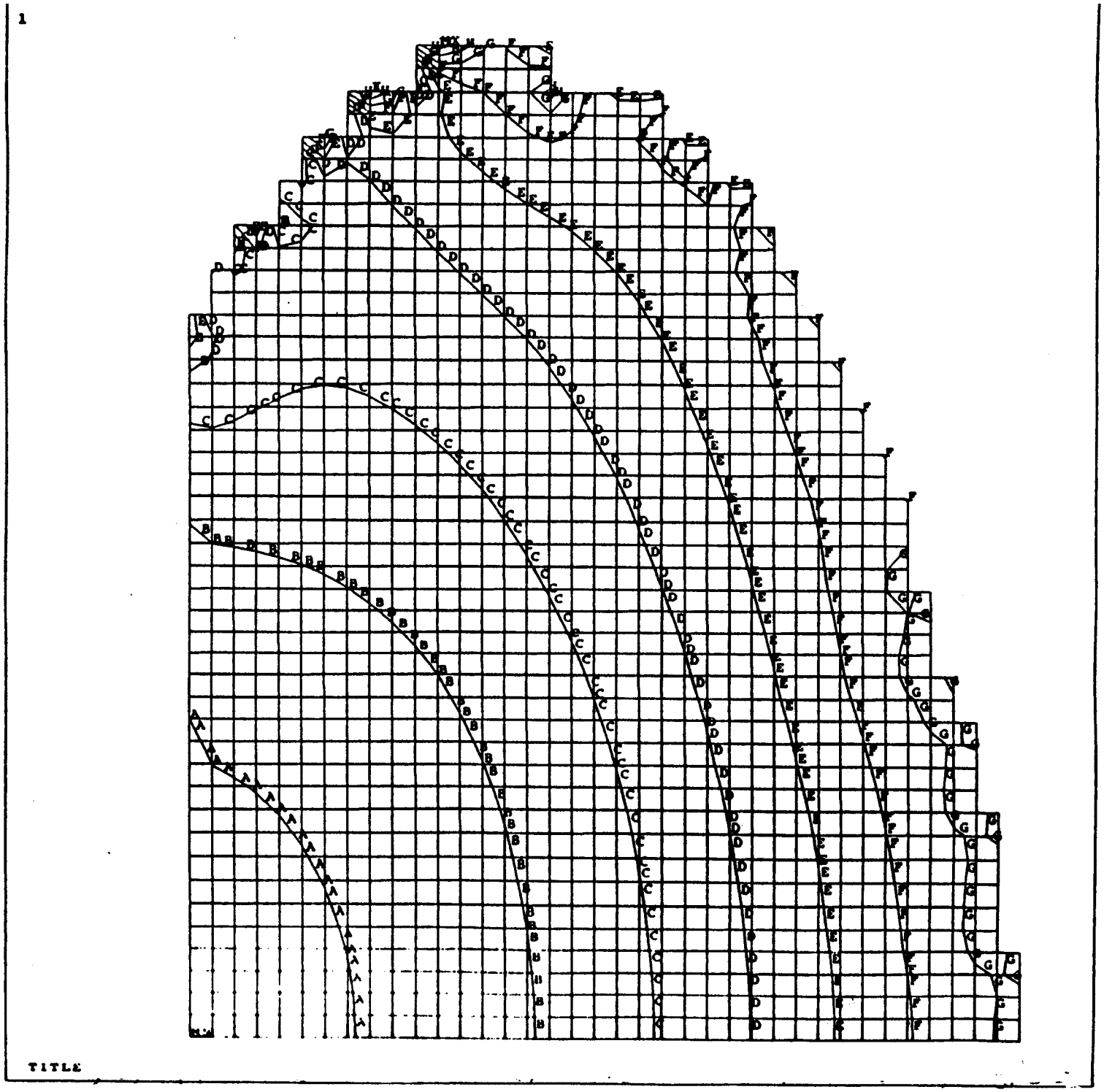

Figure 14 Distribution of the Z Component of Stress

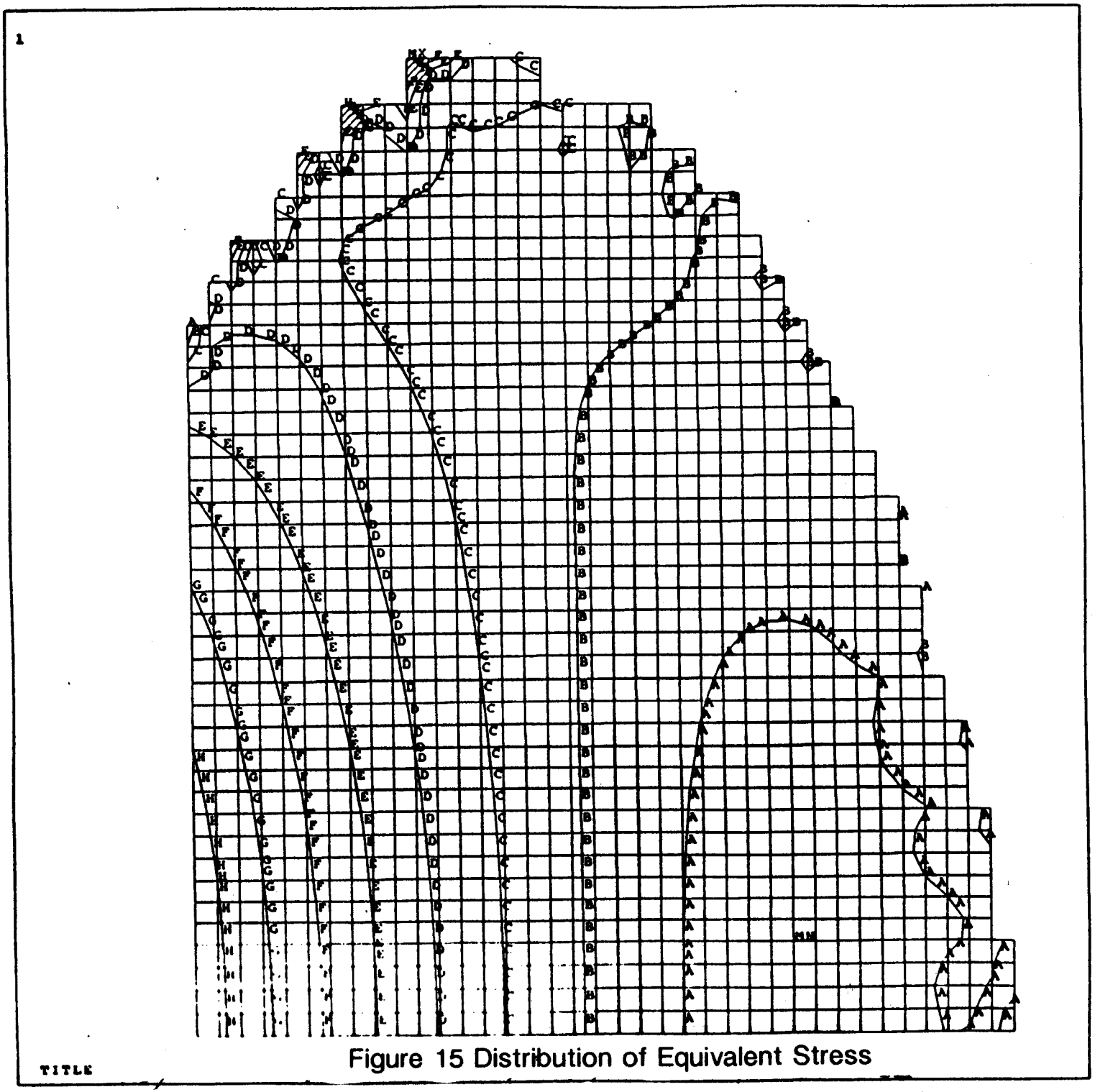

Figure 15 Distribution of Equivalent Stress